IMMUNE NETWORK

Original Article

[Check for updates]

Obesity Exacerbates Coxsackievirus Infection via Lipid-Induced Mitochondrial Reactive Oxygen Species Generation

Seong-Ryeol Kim[1],[†], Jae-Hyoung Song[1,2,†], Jae-Hee Ahn[1], Myeong Seon Jeong[3], Yoon Mee Yang[1], Jaewon Cho[1], Jae-Hyeon Jeong[1], Younggil Cha[1], Kil-Nam Kim[3], Hong Pyo Kim[4], Sun-Young Chang[4], Hyun-Jeong Ko [ID] [1,*]

[1]Department of Pharmacy, Kangwon National University, Chuncheon 24341, Korea
[2]Kangwon Institute of Inclusive Technology, Kangwon National University, Chuncheon 24341, Korea
[3]Chuncheon Center, Korea Basic Science Institute (KBSI), Chuncheon 24341, Korea
[4]College of Pharmacy, Ajou University, Suwon 16499, Korea

[lock] OPEN ACCESS

ORCID iDs
Hyun-Jeong Ko [ID]
https://orcid.org/0000-0002-3844-928X

ABSTRACT

Coxsackievirus B3 (CVB3) infection causes acute pancreatitis and myocarditis. However, its pathophysiological mechanism is unclear. Here, we investigated how lipid metabolism is associated with exacerbation of CVB3 pathology using high-fat diet (HFD)-induced obese mice. Mice were intraperitoneally inoculated with 1×10^6 pfu/mouse of CVB3 after being fed a control or HFD to induce obesity. Mice were treated with mitoquinone (MitoQ) to reduce the level of mitochondrial ROS (mtROS). In obese mice, lipotoxicity of white adipose tissue-induced inflammation caused increased replication of CVB3 and mortality. The coxsackievirus adenovirus receptor increased under obese conditions, facilitating CVB3 replication *in vitro*. However, lipid-treated cells with receptor-specific inhibitors did not reduce CVB3 replication. In addition, lipid treatment increased mitochondria-derived vesicle formation and the number of multivesicular bodies. Alternatively, we found that inhibition of lipid-induced mtROS decreased viral replication. Notably, HFD-fed mice were more susceptible to CVB3-induced mortality in association with increased levels of CVB3 replication in adipose tissue, which was ameliorated by administration of the mtROS inhibitor, MitoQ. These results suggest that mtROS inhibitors can be used as potential treatments for CVB3 infection.

Keywords: Coxsackievirus B3; Mitochondria; Reactive oxygen species; Obesity; Mitoquinone; Lipid metabolism

INTRODUCTION

With the recent surge in severe acute respiratory syndrome coronavirus-2 (SARS-CoV-2) infections worldwide, there is an increasing interest in differences in individual responses to viral infections in people with underlying health conditions. In particular, obesity is an important factor causing diabetes and high blood pressure, and viral infection in obese patients

Author Contributions

Conceptualization: Ko HJ; Data curation: Ko HJ, Kim SR, Song JH; Investigation: Kim SR, Song JH, Ahn JH, Cha Y; Funding acquisition: Ko HJ, Song JH; Formal analysis: Jeong MS, Yang YM, Jeong JH, Chang SY; Methodology: Jeong JH, Kim KN, Kim HP; Supervision: Ko HJ; Writing - original draft: Kim SR, Song JH, Cho J; Writing - review & editing: Ko HJ, Chang SY.

causes disease exacerbation. People who are obese have been reported to be more susceptible to SARS-CoV-2 infection (1). Moreover, previous studies have shown that alterations in the innate and adaptive immune responses to a number of different pathogens, such as influenza virus, increase susceptibility to infections in obese and overweight people (2,3).

Coxsackievirus B3 (CVB3) is a nonenveloped virus of the *Enterovirus* genus within the Picornaviridae family that has a single-stranded RNA genome. CVB3 infection is generally accompanied by mild symptoms such as fever, gastrointestinal disorders, headaches, and muscle pain, but can be fatal due to severe viral myocarditis (4). In addition, CVB3 also causes pancreatitis and aseptic meningitis (5). However, despite the severity of CVB3-mediated infection, the pathophysiological mechanisms of viral infection remain unclear.

RNA synthesis of many positive-stranded RNA viruses, including CVB3, occurs in the specific cytosolic structure called the replication organelle (RO), facilitating efficient viral replication and avoiding immunological detection of viral RNA. Although the regulatory mechanism of RO formation is not clearly defined, membranous invagination from the endoplasmic reticulum (ER) and mitochondria could be an initiation step (6). In addition, cells infected with certain viruses, including those of the Picornaviridae and Coronaviridae family, possess numerous double-membrane vesicles (DMVs), commonly associated with the secretory pathway (7,8). Mitochondrial herniation seems to be associated with the formation of mitochondria-derived vesicles (MDVs) as a part of DMV formation; however, the roles of MDVs in RO formation have not been identified.

Notably, mitochondrial ROS (mtROS) are an important cause of oxidative stress induced by obesity in endothelial cells. ROS play important roles in the immune system by increasing phagocytosis of intracellular pathogens and delivering danger signals. In addition, ROS are involved in cell signaling, cell survival, cell proliferation, and apoptosis. However, the overproduction of ROS can result in damage to host cells, contributing to various diseases, including respiratory, cardiovascular, neurodegenerative, and digestive diseases (9). In viral infection, ROS is associated with both beneficial and detrimental effects on cells (10). Nox4-dependent ROS generation is involved in myocardial apoptosis induced by CVB3 (11). Production of ROS is important for inducing inflammation caused by CVB3 infection (12). However, the role of mtROS generated during viral infection is obscured (13,14). Although antioxidant treatments, including mtROS inhibitors, may prevent virus replication, virus induced apoptosis, and inflammation (15,16), the association of mtROS with coxsackievirus infection in obesity has not been reported.

Accordingly, in this study, we investigated the involvement of lipid metabolism and mtROS with exacerbation of CVB3 pathology in a mouse model of obesity.

MATERIALS AND METHODS

Cell culture, viruses, and reagents

HeLa and Vero cells were purchased from American Type Culture Collection (ATCC, Manassas, VA, USA). Cells were cultured in DMEM (Corning, NY, USA), supplemented with 1% antibiotic-antimycotic solution (Invitrogen, Carlsbad, CA, USA) and heat-inactivated 10% FBS in a 37°C incubator (SANYO Electric Co, Osaka, Japan) with 5% CO_2. CVB3 (VR-30, ATCC) was used to infect Vero and HeLa cells at 37°C. The CVB3 titer was determined using

plaque assays. Mitoquinone (MitoQ) was purchased from Focus Biomolecules (Plymouth Meeting, PA, USA). MitoTEMPO and N-acetyl-L-cysteine (NAC) were purchased from Sigma-Aldrich (St. Louis, MO, USA).

Animals and virus infection

Wild-type C57BL/6 mice (8 wk) were purchased from Orient Bio Inc. (Seongnam, Korea). Mice were tagged and randomly allocated into groups (n=5/group) before any treatment or procedure. Mice were maintained in specific pathogen-free conditions at an experimental facility at Kangwon National University. All animal experiments were approved by the Institutional Animal Care and Use Committees of Kangwon National University (permit No. KW-161101-2). Mice were fed with D12492 (60 kcal% fat) or control diet D12450B (10 kcal% fat; Research Diets, Inc. New Brunswick, NJ, USA) for 2 or 4 wk. For viral infection, mice were intraperitoneally inoculated with 1×10^6 pfu/mouse of CVB3. MitoQ was intraperitoneally administered to high-fat diet (HFD)-fed mice with 2 mg/kg for 14 days starting at the day of CVB3 infection. Body temperature was measured by thermal imaging analysis using an infrared Testo 875-1i camera (Lenzkirch, Baden-Wurttemberg, Germany) while mice were conscious at 20°C.

Sulforhodamine B (SRB) assay

Antiviral activity was determined using SRB assays, as previously reported (17). The day before infection, Vero and HeLa cells were seeded in 96-well cell culture plates (Corning) at a density of 4×10^4 cells/well. After 24 h, cells were infected with CVB3 in DMEM containing heat-inactivated 1% FBS. CVB3-infected cells were incubated at 37°C with 5% CO_2, until the 70-80% cytopathic effect was achieved. After 48 h, cell culture plates (96-well) containing samples were washed with 1× PBS and fixed with 100 μL/well 70% ice-cold acetone for 30 min at −20°C. Following removal of acetone, plates were dried in a drying oven at 70°C. Thereafter, dried cells in each well were stained with 0.4% (w/v) SRB (Sigma-Aldrich)/1% acetic acid for 20 min. Precipitated SRB crystals were dissolved at 100 μL/well in 10 mM unbuffered tris-based solution. The blank absorbance was read at 650 nm, and the sample absorbance was read at 562 nm using a SpectraMax i3 microplate reader (Molecular Devices, Palo Alto, CA, USA).

Quantitative RT-PCR (RT-qPCR)

Total RNA was isolated using a QIAamp Viral RNA Mini Kit (Qiagen, Valencia, CA, USA). RT-qPCR was performed as previously described (18). We used the following primers: EV-NCR sense, 5′-CCGGCCCCTGAATGCGG-3′ and EV-NCR antisense, 5′-ATTCTTTAATTGTCACCATAAGCAGCCA-3′; monkey β-actin-sense, 5′-AAGGATTCATATGTGGGCGATG-3′ and monkey β-actin-antisense, 5′-TCTCCATGTCGTCCCAGTTGGT-3′; human β-actin-sense, 5′-CCATCATGAAGTGTGACGTGG-3′ and human β-actin-antisense, 5′-GTCCGCCTAGAAGCATTTGCG-3′ and mouse β-actin-sense, 5′-GGCTGTATTCCCCTCCATCG-3′ and mouse β-actin-antisense, 5′-CCAGTTGGTAACAATGCCATGT-3′. The conditions for PCR amplification were as follows: initial denaturation at 95°C for 3 min, followed by 35 cycles of 95°C for 30 s, 60°C for 30 s, 72°C for 30 s, and a final extension at 72°C for 10 min. To evaluate the ability of TaqMan to discriminate between the positive and negative CVB3 RNA strands, we used a customized AccuPower Coxsackievirus B3 Real Time RT-PCR Kit (Bioneer, Deajeon, Korea).

Histological analysis

The tissues from CVB3-infected mouse were fixed with 4% formaldehyde (Masked Formalin; DANA Korea, Incheon, Korea) for overnight at 20°C. The CVB3-infected mouse tissues were

dehydrated in ethanol and xylene, then embedded in paraffin. Tissue section were sliced into 5 μm, and stained with H&E. The stained tissues were evaluated to determine the degree of inflammation under light microscope (100×) (Olympus CX41; Olympus, Tokyo, Japan).

Western blot analysis

Total protein lysates from cells or tissues were prepared by sonication with PRO-PREP™ Protein Extraction Solution (iNtRON Biotechnology, Seongnam, Korea). Protein levels were determined using a Pierce™ BCA Protein Assay Kit (Thermo Fisher Scientific, MA, USA). Equivalent amounts of protein were separated by sodium dodecyl sulfate polyacrylamide gel electrophoresis and transferred to membranes. The membranes were subsequently incubated with primary Abs, including anti-coxsackievirus and adenovirus receptor (CAR) Abs (Santa Cruz Biotechnology, Dallas, TX, USA) and anti-β-actin Abs (cat. No. SC-47778; Santa Cruz Biotechnology) for 16 h at 4°C. Thereafter, secondary Abs, including goat anti-rabbit IgG (H+L)-HRP conjugate (Bio-Rad Laboratories, Hercules, CA, USA) and goat anti-mouse IgG F(ab′)2, polyclonal Abs (HRP conjugate) (Enzo Life Sciences, Farmingdale, NY, USA), were added for 1 h at 20°C. Proteins were detected using a femtoLUCENT PLUS-HRP Kit (G-Biosciences, Maryland Heights, MO, USA) and visualized with an ImageQuant LAS 4000 mini system (Cytiva, Marlborough, MA, USA). Chemiluminescence intensity was analyzed using Image J software (NIH, Bethesda, MD, USA).

Surgical lipectomy

Surgical lipectomy was performed as previously reported (19). In surgical removal of epididymal white adipose tissue (eWATx) mice, the test was carefully performed to avoid damage to the testicular blood supply. Both left and right epididymal white adipose tissue (eWAT) fat pads were surgically removed via a mid-abdominal incision. For the sham eWATx group, both left and right eWAT fat pads were pulled; however, they remained intact and were placed back into the abdominal cavity.

Measurement of intracellular ROS

Vero cells were seeded in 24-well cell culture plates at a density of 1.5×10^5 cells/well 1 day prior to the experiment. After 24 h, the remaining medium was removed, and 0.1% BSA only or 50 μM oleic acid (OA) in 0.1% BSA was added. Cells were further incubated for 24 h, washed twice with 1× PBS, and infected with CVB3 for 1 h in DMEM containing 1% heat-inactivated FBS. Cells were washed twice with 1× PBS and stained with 5 μM MitoSOX (Invitrogen) for 30 min at 37°C and 5% CO_2. Thereafter, cells were washed twice with 1× PBS and fixed with 4% paraformaldehyde. Cells were assessed using FACSVerse instruments (BD Bioscience, San Diego, CA, USA), and the data were analyzed using FlowJo (FlowJo, Ashland, OR, USA).

Quantitative immunohistochemistry

White adipose tissue (WAT) specimens from mice were fixed with 4% formaldehyde for 16 h at 20°C. Fixed WAT tissues were dehydrated in ethanol and xylene and subsequently embedded in paraffin. Tissues were sliced into 5-μm-thick sections and stained with primary Abs (F4/80 Monoclonal Ab [BM8]; eBioscience, San Diego, CA, USA). Subsequently, samples were stained with rat-specific HRP-conjugated secondary Abs (R&D Systems, Minneapolis, MN, USA).

Immunofluorescence

Vero cells (2×10^5 cells/well) were seeded in 6-well culture plates (Corning/Falcon). After 24 h, cells were treated with or without 100 μM OA (0.1% BSA) and subsequently incubated for 24 h

at 37°C with 5% CO_2. Cells were infected with CVB3 for 12 h, fixed with 4% paraformaldehyde at 20°C for 10 min, permeabilized with 0.25% Triton-X 100, blocked with 5% skim milk for 1 h, and finally stained with primary Abs, including anti-CVB3 Abs (clone 280-5F-4E-5E; Merck-Millipore, Burlington, MA, USA), anti-TOM20 Abs (Cell Signaling Technologies, Denver, MA, USA), and anti-pyruvate dehydrogenase E2/E3bp Abs (Abcam, Cambridge, MA, USA) at 20°C for 2 h. Following washing with PBS, cells were stained with secondary Abs, including anti-mouse IgG (H+L), F(ab′)2 fragment (Alexa Fluor 488 conjugate), goat anti-rabbit IgG H&L (Alexa Fluor 488) (Abcam), or donkey anti-Mouse IgG (H+L) (Alexa Fluor 555) (Thermo Fisher Scientific), for 2 h at 20°C. Thereafter, cells were mounted with 4′,6-diamidino-2-phenylindole and images were viewed under a confocal laser scanning microscope LSM880 (Carl Zeiss, Göttingen, Germany) at the Central Laboratory of Kangwon National University and Zen software (Carl Zeiss).

Transmission electron microscopy (TEM)

Vero cells (5×10^6 cells/well) were seeded in Falcon 100 mm cell culture dishes (Corning). After 24 h, cells were treated with or without 100 μM OA (0.1% BSA) and incubated for 24 h at 37°C in a 5% CO_2 incubator. Cells were infected with CVB3 for 12 h, fixed with 0.1% glutaraldehyde and 2% paraformaldehyde in phosphate buffer (pH 7.4) for 1 h at 4°C, and subsequently post-fixed with osmium tetroxide for 40 min at 4°C. Samples were dehydrated in a graded ethanol series, treated with a graded propylene oxide series, and embedded into Epon (TED Pella Inc., CA, USA). Thereafter, cells were sliced into ultra-thin sections (80 nm) and placed on copper grids. Samples were stained with uranyl acetate and lead citrate and observed using a transmission electron microscope (JEM-2100F; Jeol, Tokyo Japan) at 200 kV (KBSI Chuncheon Center).

Statistical analysis

All results are expressed as means±SEMs and were analyzed using one-way analysis of variance followed by Newman-Keuls multiple comparison test. Differences between groups were assessed using unpaired 2-tailed Student's *t*-tests. Statistical analyses were performed using GraphPad Prism software version 5 (GraphPad Software, La Jolla, CA, USA). Results with p-values of less than 0.05 were considered statistically significant.

RESULTS

Mice fed a HFD showed increased severity of CVB3 infection

To assess the effects of HFD-induced obesity on CVB3 infection, mice fed a regular diet (RD) or HFD were infected with CVB3. Mice fed the HFD showed a significant reduction in survival after CVB3 infection compared with RD-fed mice, and mice fed an HFD for 4 wk had a lower survival rate than mice fed an HFD for 2 wk following CVB3 infection (**Fig. 1A**). In addition, the body temperature of HFD-fed mice decreased significantly compared with that of RD-fed mice at 3 days after CVB3 infection (**Fig. 1B**).

Because CVB3 initially replicates in the pancreas following intraperitoneal infection (20), we further screened several other tissues to assess tissue-specific replication (as determined by negative-strand viral RNA) and viral burden (as determined by positive-strand viral RNA) of CVB3 in mice. The replication of CVB3 facilitated in the pancreas of HFD-fed mice was higher on day 1 following CVB3 infection as compared to that of RD-fed mice. Notably, CVB3 replication was significantly increased in the WAT of HFD-fed mice on day 2 following viral
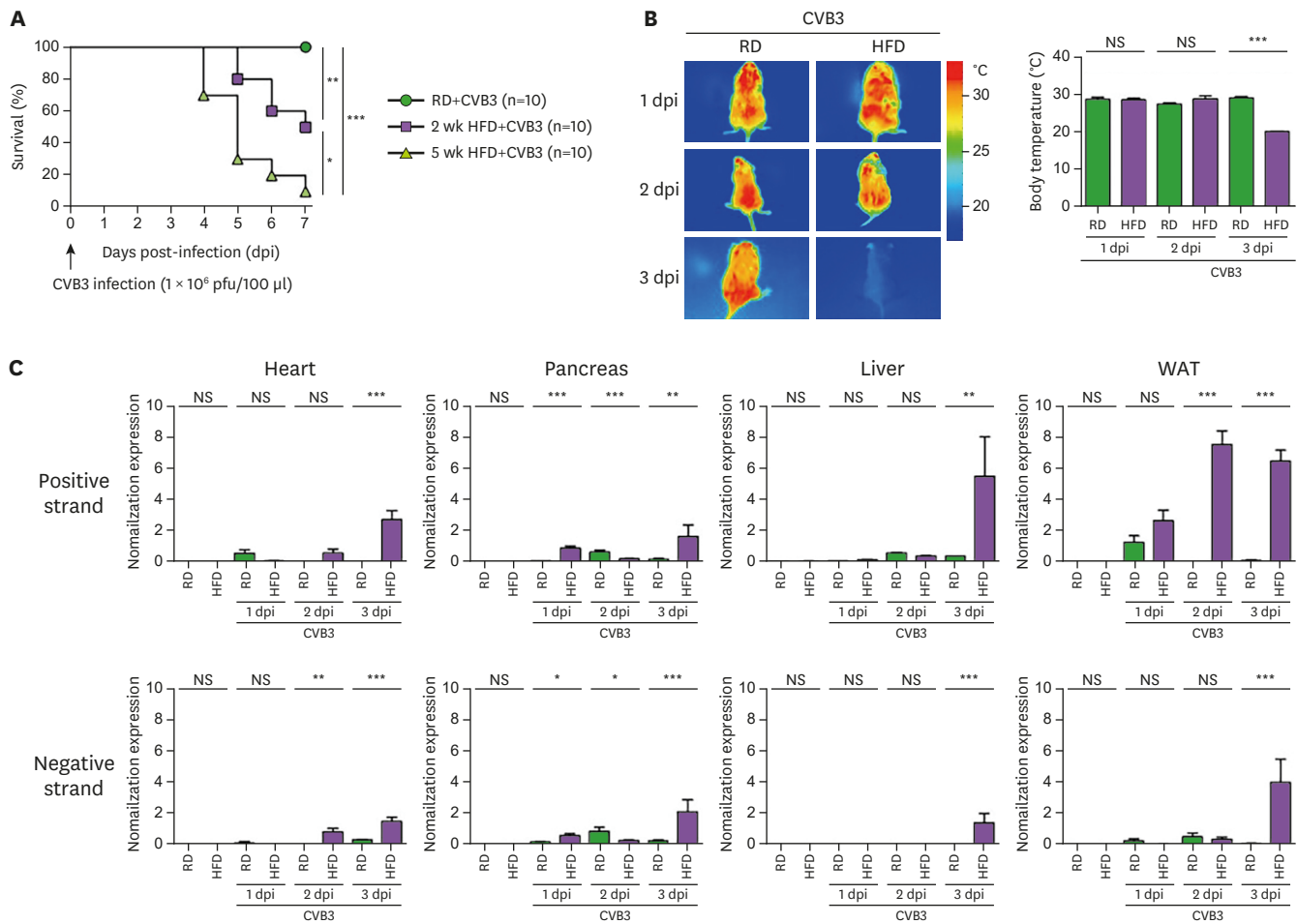
Figure 1. HFD-induced obesity increased mortality and morbidity in CVB3-infected mice. Eight-week-old male C57BL/6 mice were divided into three groups (n = 10 per group), and each group of mice was fed a RD for 4 wk, HFD for 2 wk, or HFD for 4 wk. (A) Survival in the CVB3-infected group was monitored for 7 days after intraperitoneal CVB3 (1×10⁶ pfu/mouse) injection. (B) The body temperature of mice was measured for 1–3 days post-infection. (C) Normalized expression of the positive-strand and negative-strand CVB3 gene (5′-UTR) was determined by real-time PCR 1–3 days post-infection. Data are expressed as means±SEMs. NS, not significant.
*p<0.05, **p<0.01, and ***p<0.001.

infection. This data suggests that WAT in HFD-fed mice may be important place for CVB3 replication (**Fig. 1C**). In addition, we confirmed that the CVB3 burden in the pancreas, WAT, liver, and heart was profoundly increased in HFD-fed mice compared with RD-fed mice on day 3 after infection. Collectively, these results suggested that CVB3 replicated in several tissues, including the WAT, under obese conditions.

Obesity increased lipotoxicity and inflammation in the WAT of CVB3-infected mice

In order to further understand the enhanced severity of CVB in HFD-fed mice, we examined CVB3-infected obese mice for diagnostic necropsy. Gross anatomical analysis of abdominal organs in mice suggested the presence of lipotoxicity in the WAT of HFD-fed mice following CVB3 infection (**Fig. 2A**). H&E staining of WAT revealed that cell infiltration involved adipose tissue macrophage (ATM)-like cells expressing F4/80 (**Fig. 2B and C**). More ATM-like cells infiltrated into eWAT of HFD-fed mice at 3 days after CVB3 infection compared to RD-fed mice. In contrast, we did not observe any marked difference in the pancreas of RD- and HFD-fed mice on day 3 post-infection as both groups showed similar levels of acinar cell

IMMUNE NETWORK
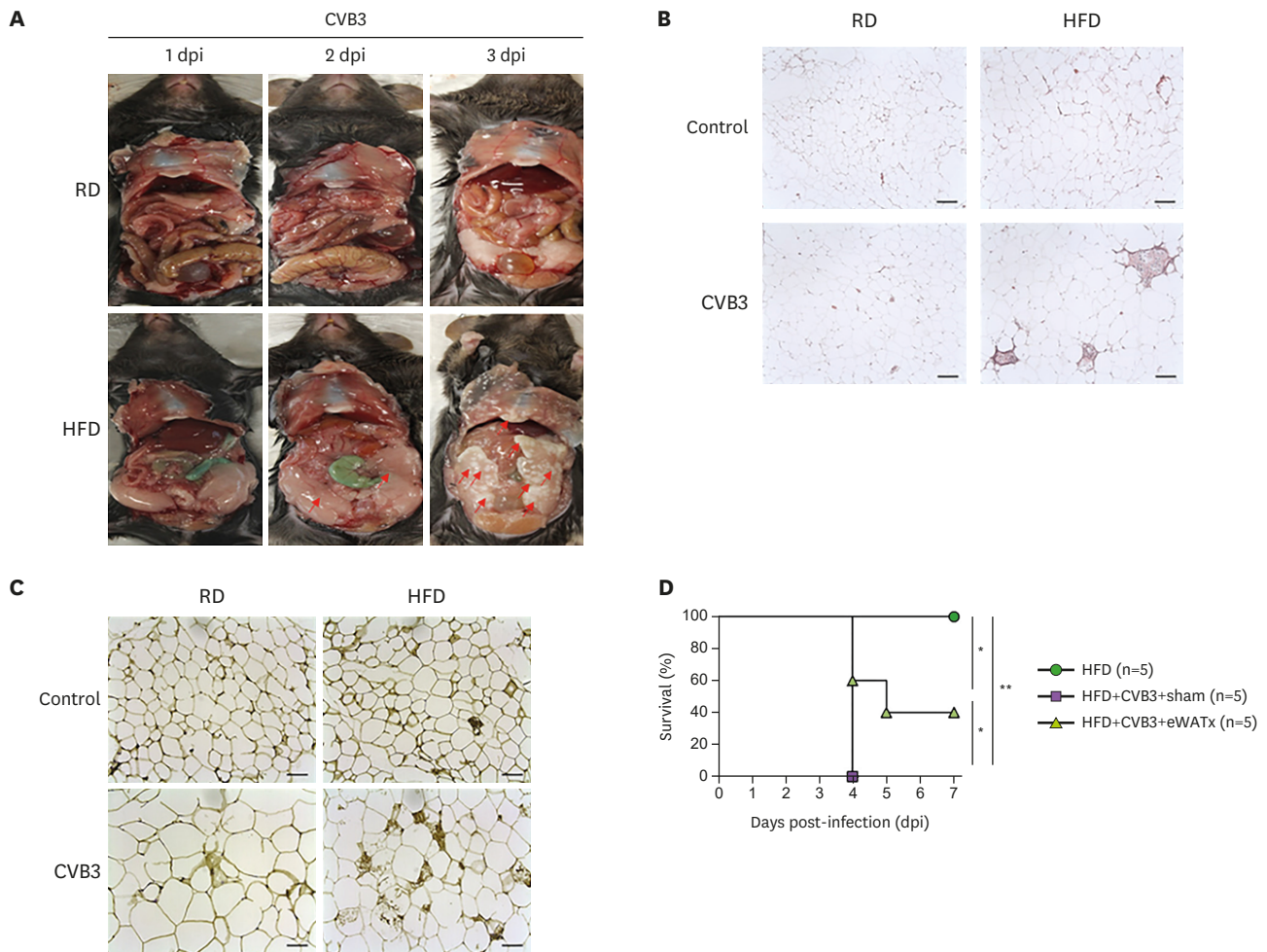
Figure 2. HFD-fed obese mice showed accelerated acute inflammation and lipotoxicity in WAT following CVB3 infection. Groups of mice were fed a RD or HFD for 4 wk and intraperitoneally infected with CVB3 (1×10^6 pfu/mouse). (A) Representative images of WAT at 1–3 days post-infection. Lipocytoxicity of WAT as indicated by red arrows. (B) Representative H&E staining results for WAT. (C) Immunohistochemical staining for F4/80 expression in WAT at 3 days post-infection. (D) eWAT was surgically removed (eWATx) from obese mice fed an HFD for 4 wk, and the mice were intraperitoneally infected with CVB3 (1×10^6 pfu/mouse). Survival of mice was monitored for 7 days following CVB3 infection (n = 5/group). Data are expressed as means±SEMs.
$^*p<0.05$ and $^{**}p<0.01$.

hypochromicity and inflammatory cell infiltration (**Supplementary Fig. 1A**). Similarly, there were no pathological differences in the livers and hearts of both groups (**Supplementary Fig. 1B and C**). To assess whether the WAT was critical for CVB3-induced mortality in HFD-fed mice, we surgically removed the eWAT of mice (eWATx mice). The survival of eWATx mice was significantly higher than that of non-eWATx mice following CVB3 infection (**Fig. 2D**). These data indicated that the increased mortality of CVB3-infected obese mice was associated with severe inflammation in WAT.

OA treatment increased CVB3 replication *in vitro*

Fatty acids are known to enhance replication of several viruses, such as influenza virus (21) and Singapore grouper iridovirus (22). However, the relationship between fatty acids and CVB3 replication has not yet been reported. To investigate the role of fatty acids in CVB3 replication, we treated Vero cells with OA, the main free fatty acid of the HFD, to induce lipid accumulation in cells prior to CVB3 infection. We measured CVB3 gene expression levels using RT-qPCR to assess the effects of OA accumulation on host cells and CVB3 infection replication. The levels

IMMUNE
NETWORK
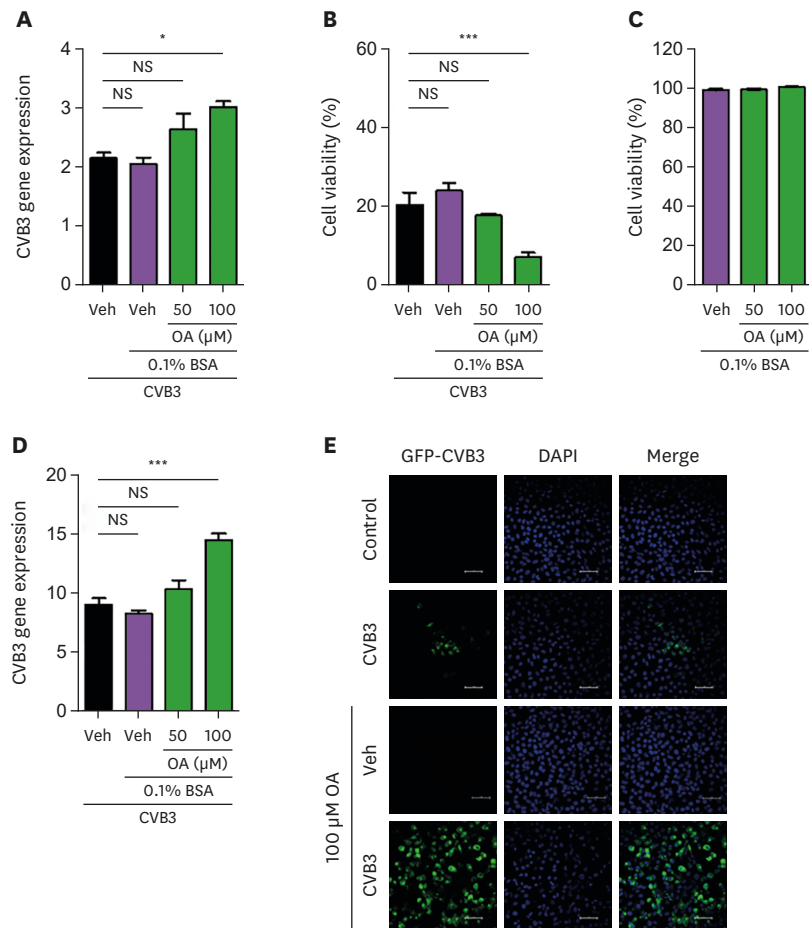
Figure 3. OA increased CVB3 replication *in vitro.* (A) Vero cells were pretreated for 24 h with 50 or 100 μM OA noncovalently conjugated with 0.1% BSA and infected with CVB3 at a MOI of 10 for 24 h. Normalized CVB3 gene expression in Vero cells was determined by real-time PCR. (B) Vero cells were treated with the indicated concentrations of OA with the virus for 48 h. (C) Vero cells were treated with the indicated concentrations of OA without the virus for 48 h. Viability of Vero cells was measured using SRB assays. (D) HeLa cells were pretreated for 24 h with 50 or 100 μM OA noncovalently conjugated with 0.1% BSA and infected with CVB3 at an MOI of 10 for 24 h. Normalized expression of the CVB3 gene in HeLa cells was determined by real-time PCR. (E) Vero cells were pretreated for 24 h with 100 μM OA noncovalently conjugated with 0.1% BSA and were infected with CVB3 at an MOI of 10 for 24 h. Representative images stained with anti-CVB3 Ab (green). All figures are representative examples of experiments performed in triplicate. Data are expressed as means±SEMs.
Veh, vehicle; NS, not significant; MOI, multiplicity of infection.
[*]p<0.05, and [***]p<0.001.

of CVB3 positive-sense, single-stranded RNA in Vero cells were significantly increased with 100 μM OA (0.1% BSA) treatment for 24 h (**Fig. 3A** and **Supplementary Fig. 2**). In addition, OA treatment increased CVB3-mediated cytotoxicity (**Fig. 3B**), whereas 100 μM OA (0.1% BSA) treatment alone did not induce cytotoxicity in Vero cells at 48 h (**Fig. 3C**). We also confirmed that OA accumulation in HeLa cells increased CVB3 replication (**Fig. 3D**). The number of CVB3-GFP puncta representing viral gene expression in Vero cells increased significantly after OA treatment (**Fig. 3E**). Collectively, these results demonstrated that increased replication of CVB3 was associated with accumulated OA in host cells.

Valsartan treatment did not inhibit CVB3 infection upon OA treatment

The CAR plays important roles in the entry of both coxsackie B viruses and adenoviruses into host cells (23). Because CAR expression is increased in obese adipose tissue (24), we assessed
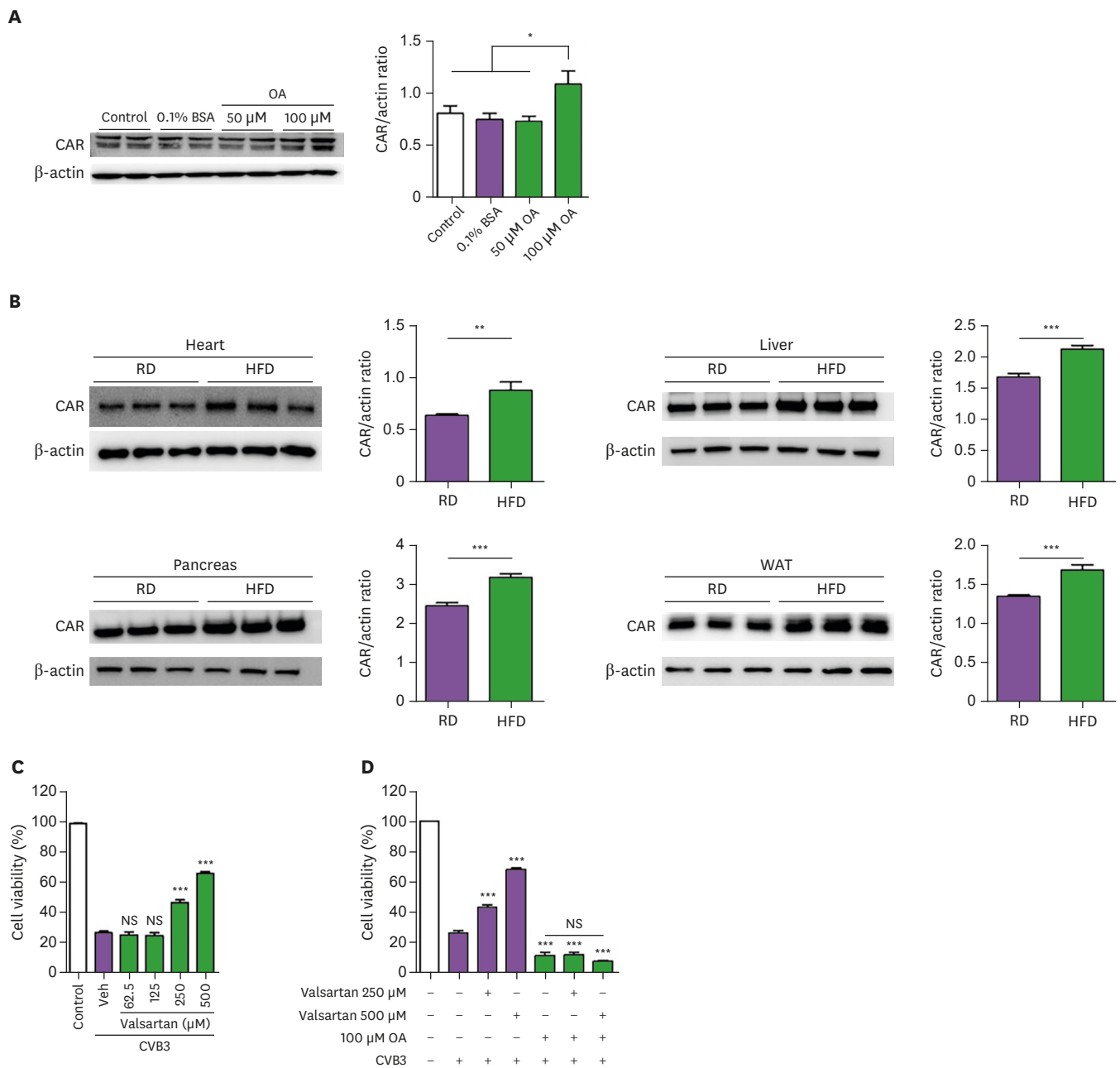
Figure 4. CVB3-induced cytotoxicity enhanced by OA and a HFD did not recover by valsartan treatment. (A) HeLa cells were treated with 0.1% BSA, 50 μM OA in 0.1% BSA, or 100 μM OA in 0.1% BSA for 24 h. The expression of CAR and β-actin was determined from cell lysates using western blot analysis. (B) Mice were fed a RD or HFD for 4 wk, and the expression of CAR protein in the heart, liver, pancreas, and WAT of mice was determined by western blot analysis. (C) Vero cells were infected with CVB3 at a MOI of 10 and treated with the indicated concentrations of valsartan for 48 h. Cell viability was measured using SRB assays. (D) Vero cells were pretreated with 100 μM OA in 0.1% BSA for 24 h and subsequently infected with CVB3 at an MOI of 10 in the presence of 250 or 500 μM valsartan for 48 h. All figures are representative examples of experiments performed in triplicate. Data are expressed as means±SEMs.
NS, not significant; Veh, vehicle; MOI, multiplicity of infection.
[*]p<0.05, [**]p<0.01, and [***]p<0.001.

changes in CAR expression in Hela cells following OA treatment. CAR expression in HeLa cells increased following 100 μM OA (0.1% BSA) treatment (**Fig. 4A**). Notably, the expression levels of CAR in the heart, pancreas, liver, and WAT increased significantly in HFD-fed mice compared with those in RD-fed mice (**Fig. 4B**).

Valsartan is a well-known antihypertensive drug that exhibits antiviral activity against CVB3 in association with its effect on downregulating CAR in human endothelial cells (25). Similarly, Vero cells pretreated with 250 or 500 μM of valsartan for 48 h showed significant antiviral activity against CVB3, as demonstrated by reduced CVB3-mediated cytotoxicity (**Fig. 4C**). However, valsartan did not significantly reduce the enhanced cytotoxicity of CVB3 infected cells with OA accumulation (**Fig. 4D**). These results suggested that the upregulation of CAR by OA treatment was independent from the increased CVB3 replication in lipid-accumulated host cells.

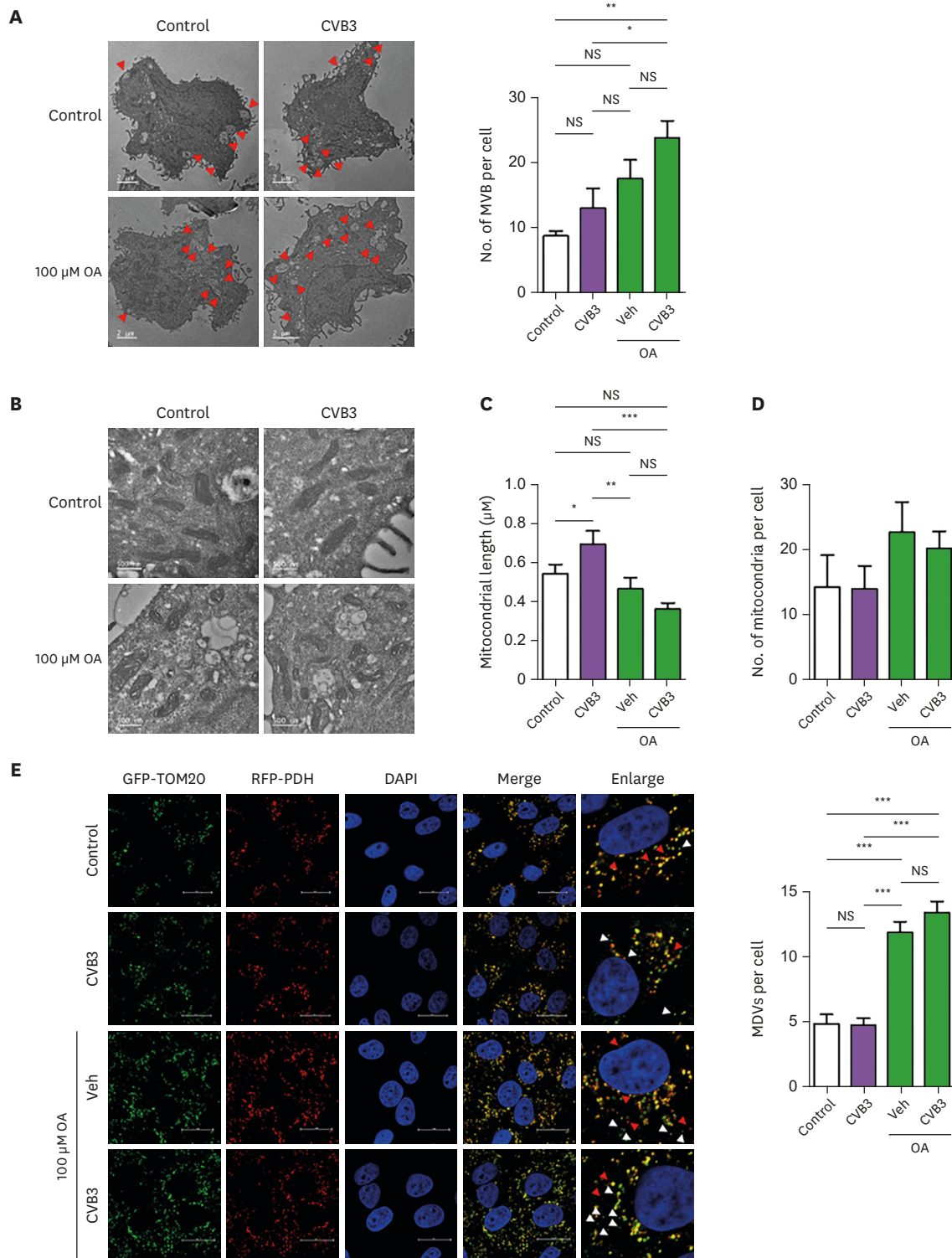## OA treatment was correlated with RO formation upon CVB3 infection

MDVs are cargo systems that deliver mitochondrial contents, such as membrane components and mtDNA, to other intracellular organelles, including multivesicular bodies (MVBs) or late endosomes (26). We hypothesized that the RO of CVB3 could be derived from MDVs because MDVs can be transferred to MVBs (27,28) and MVB-like structures found during viral infection was similar to ROs (29). Assessment of TEM images of thin sections of OA-treated and untreated Vero cells showed that the number of MVBs was higher in Vero cells treated with OA than in untreated cells (**Fig. 5A**). Previous reports showed that OA treatment induced mitochondrial dysfunction in human umbilical vein endothelial cells (30). Similarly, OA treatment induced sequential mitochondrial modifications (**Fig. 5B**) including a decrease in average length (**Fig. 5C**). However, OA did not alter the number of mitochondria compared with that in untreated cells (**Fig. 5D**). MDVs can be identified by analysis of the mitochondrial marker translocase of the outer mitochondrial membrane (TOM20) and mitochondrial matrix protein (PDH) (31) and can be discriminated for the mitochondrial markers of PDH$^+$/TOM20$^-$ (matrix) or TOM20$^+$/PDH$^-$ (outer mitochondrial membrane) by selective and high enrichment (32,33). We also confirmed that OA treatment of Vero cells increased MDV formation, as determined by analysis of TOM20$^+$ or PDH$^+$ enriched vesicles (**Fig. 5E**) (34). This finding suggested that OA treatment triggered mitochondrial dysfunction with enhanced MDV formation, which in turn provided a nest for CVB3 replication.

## mtROS induced by OA treatment increased CVB3 replication

Previous reports have suggested that free fatty acids, such as palmitic acid and OA, can increase the generation of mtROS in various cells, including endothelial and epithelial cells (35). Thus, we assessed the level of mtROS using MitoSOX Red staining followed by flow cytometry. The level of mtROS increased in Vero cells treated with OA (0.1% BSA) compared with that in untreated cells. This increase was blocked by treatment with 50 μM MitoTEMPO, which inhibits mtROS (**Fig. 6A**). A previous study suggested that the replication of several viruses, including influenza (13), enterovirus 71 (36), and respiratory syncytial virus (16), is influenced by increased mtROS generation. Thus, we hypothesized that increased CVB3 replication upon OA treatment may be related to increased mtROS production. Notably, the reduced survival of OA-pretreated Vero cells following CVB3 infection was significantly increased by MitoTEMPO treatment (**Fig. 6B**). Similarly, CVB3 gene expression increased upon OA treatment and decreased significantly with MitoTEMPO treatment (**Fig. 6C**). In contrast, CVB3-induced cytotoxicity in OA-pretreated cells did not improve following treatment with NAC, which inhibits cytosolic ROS (**Supplementary Fig. 3**), suggesting that the increase in mtROS upon OA treatment was crucial for enhanced CVB3 replication *in vitro*.

MitoQ treatment protected mice from CVB3 infection

MitoQ specifically inhibits mtROS accumulation *in vivo* (37) and exhibits antiviral activity against respiratory syncytial virus in human alveolar epithelial cells (16). Therefore, we next evaluated the antiviral activity of MitoQ *in vivo*. Mice were intraperitoneally infected

Figure 5. RO formation induced by CVB3 infection was correlated with OA treatment conditions. Vero cells were pretreated with 100 µM OA in 0.1% BSA for 24 h and infected with CVB3 at a MOI of 10 for 12 h. (A) Formation of MVBs (red arrow) was evaluated using transmission electron microscopy. (B-D) Mitochondrial length (C) and number of mitochondria (D) were quantitatively analyzed in Vero cells as indicated. (E) Cells were subsequently immunostained for detection of TOM20 (green), PDH2/3 bp (red), and nuclei (blue). The numbers of TOM20+ MDVs (white arrow) or PDH+ MDVs (red arrow) per cell were quantified using immunofluorescence imaging. Data are expressed as means±SEMs.
NS, not significant; Veh, vehicle; MOI, multiplicity of infection.
*p<0.05, **p<0.01, and ***p<0.001.
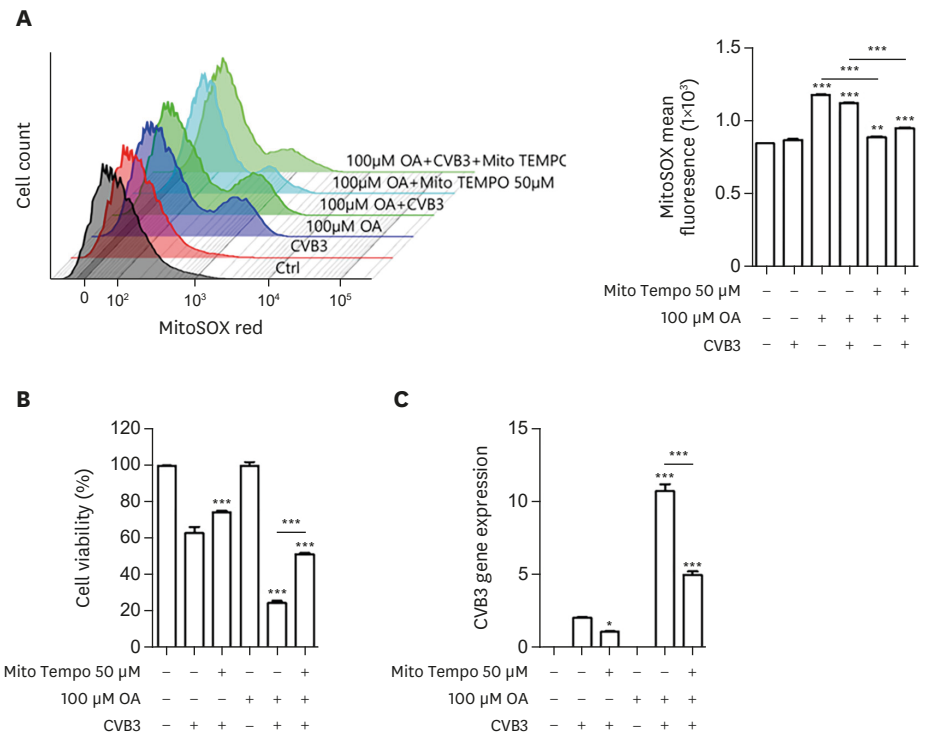
Figure 6. Inhibition of mitochondrial ROS reduced CVB3 replication. (A) Vero cells were pretreated with 100 μM OA in 0.1% BSA for 24 h and infected with CVB3 at a MOI of 10 for 1 h. (A) Cells were stained with 5 μM MitoSOX and analyzed by flow cytometry. (B, C) Vero cells were pretreated for 24 h with 100 μM OA in 0.1% BSA and infected with CVB3 (MOI 10) in the presence or absence of 50 μM Mito Tempo for 48 h. (B) Normalized CVB3 gene expression was determined by real-time PCR. (C) Cell viability was measured using SRB assays. All figures are representative examples of experiments performed in triplicate. Data are expressed as means±SEMs.
MOI, multiplicity of infection.
$^{*}p<0.05$, $^{**}p<0.01$, and $^{***}p<0.001$.

with CVB3, and MitoQ was administered once every day for 14 days starting on the day of infection. HFD-fed mice in the CVB3 infection group treated with vehicle died within 5 days after infection, whereas more than 50% of mice treated with MitoQ survived until 14 days post-infection (**Fig. 7A**). In addition, MitoQ treatment ameliorated the infiltration of ATM-like cells in the WAT of HFD-fed mice at 3 days after CVB3 infection (**Fig. 7B and C**) and inhibited CVB3 gene expression in WAT. Collectively, these results suggested that increased mtROS induced by HFD feeding may aggravate CVB3 infection in mice and that inhibition of mtROS using MitoQ was attributed to its antiviral effects against CVB3 in obesity.

DISCUSSION

Obesity is a major risk factor for infections, and the incidence rates of several infections have been shown to be increased in obese individuals (38,39). In particular, obese individuals are more susceptible to various viral infections, including influenza A virus, rhinovirus, and severe acute respiratory syndrome coronavirus, compared with nonobese individuals (40). Several studies have shown that obesity impairs immune responses to viral infections (41). For example, in obese mice, influenza virus reduces the levels of antiviral cytokines, such as IFN-α and IFN-β, which are essential for infection control (42). Few studies have addressed cell-intrinsic factors regulating viral infection in association with obesity.
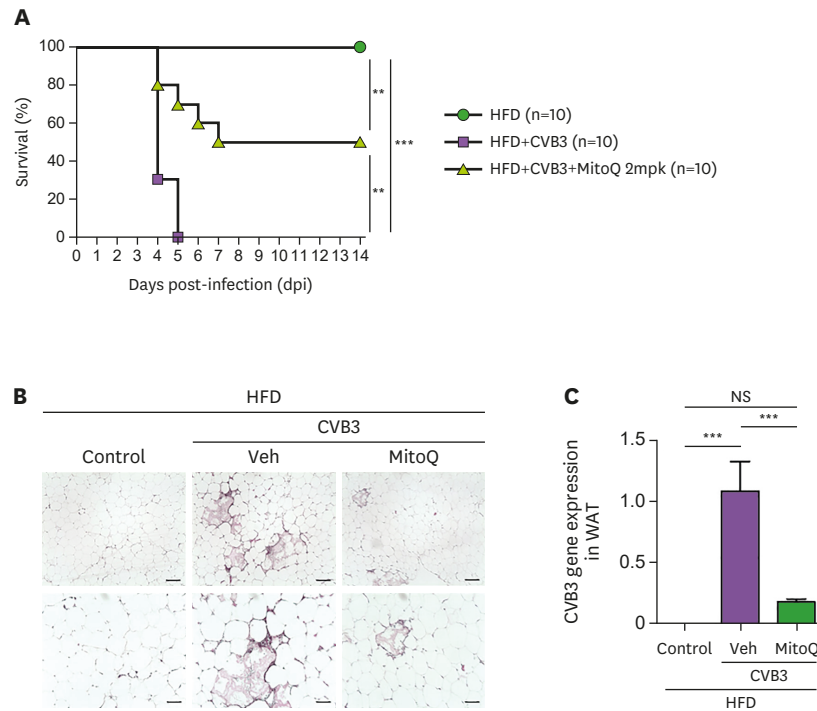
Figure 7. MitoQ had therapeutic effects on obese mice infected with CVB3. Mice were fed a HFD for 4 wk. Mice were infected with CVB3 at 1×10⁶ pfu/mouse, and 2 mg/kg MitoQ was intraperitoneally administered. (A) Survival was monitored for 14 days (n=10/group). (B) Representative histology staining of WAT 3 days post-infection. (C) Normalized CVB3 gene expression in the pancreas was determined by PCRRT-PCR 3 days post-infection. Data are expressed as means±SEMs.

NS, not significant; Veh, vehicle.

**p<0.01, and ***p<0.001.

In the current study, we found that obese mice fed an HFD were more susceptible to CVB3 infection and showed increased mortality. Notably, increased mtROS was detected in MDVs of obese-conditioned host cells, and inhibition of mtROS using MitoQ successfully ameliorated HFD-induced CVB3 infection in the WAT and enhanced the survival rates of CVB3-infected obese mice. Collectively, our findings demonstrated that obesity increased the severity of CVB3 infection, which induced lethality in mice. Thus, we proposed that mtROS inhibitors could be adapted to ameliorate CVB3 infection, particularly in the context of obesity.

CVBs can cause both acute and chronic infectious diseases in humans, are the most common causes of infectious myocarditis (43), and are known to cause pancreatitis and aseptic meningitis (5,44). However, CVB3 replication in the WAT of mice has not been reported. In the current study, we found that the WAT was another important replication site for CVB3 and may be associated with increased disease severity in obese mice following CVB3 infection.

For CVB3 replication, the generation of the RO, a specialized membranous complex inside eukaryotic cells, is required for CVB3 replication (45). Enteroviruses trigger the recruitment of lipid droplets to provide lipids required for the development of ROs (46). Viral protein 3A of enteroviruses is a critical viral factor triggering the formation ROs via the interaction of the phosphatidylinositol kinase PI4KB and the sterol transporter OSBP to elicit the shuttling of lipids between lipid droplets and ROs (47). Free fatty acids in cells are stored as lipid droplets and are associated with metabolic diseases, such as obesity and diabetes (48). Obesity can

induce lipid-mediated metabolic or cell signaling malfunction, resulting in increased RO formation, which has advantages for CVB3 replication.

Lipids are important constituents of the plasma membrane and other cellular compartments (49). OA and palmitic acid increase mtROS generation in endothelial cells (35); thus, we confirmed that OA treatment in Vero cells significantly increased mtROS generation. In several studies, infection with many viruses, including hepatitis B virus, hepatitis C virus (HCV), HIV, respiratory syncytial virus, and influenza virus, was found to trigger mtROS production (50). Additionally, ROS produced after viral infection can help fight against viral infections; however, antioxidants exhibit antiviral effects against several viruses by reducing oxidative stress (51). In this study, MitoTEMPO inhibited CVB3 replication in obese-conditioned Vero cells by reducing the level of mtROS. This result implied that lipid-treated conditions exacerbated mtROS production following viral infection and further increased the formation of MDVs, which in turn enhanced viral replication.

MDVs resembles DMVs, which are sites of viral RNA replication for HCV (52) and provide substantial support for viral RNA replication in enteroviruses (53). MDVs are generated during oxidative stress (54); thus, mtROS can be a trigger for MDV formation. Because mtROS-containing MDVs control bacteria-containing phagosomes (55), mtROS in MDVs may be involved in CVB3 infection. We hypothesized that, in virus-infected cells, MDVs could reach MVBs, together with DMVs or ROs, and then eventually be expelled from cells as extracellular vesicles and virus particles (28). Incidentally, MVBs are known to play important roles in the trafficking of several viruses, including vesicular stomatitis virus (56) and HIV-1 (57). However, the roles of MDVs in the replication of CVB3 infection have not been elucidated. Notably, blockade of mtROS inhibits CVB3 replication. We presumed that MDVs induced by mtROS may facilitate MVB or RO formation, resulting in tissue tropism of CVB3. However, the association of mitochondrial herniation and lipid droplets for RO formation remains unclear, and further studies are required.

MitoQ and MitoTEMPO were originally designed as mitochondria-targeted antioxidants that block mtROS production (58,59); these reagents have been used in the context of several human diseases and do not induce toxicity (60). Mitochondrial superoxide and ROS production by mitochondrial dysfunction in WAT are associated with obesity, hepatosteatosis, and subsequent complications; accordingly, inhibition of mtROS may be a novel treatment strategy for obesity-associated disorders (37). However, antioxidant drugs differ in the ability to reduce virus replication. NAC inhibits hepatitis B virus replication (61), but does not prevent apoptosis in cytopathic human rhinovirus and bovine viral diarrhea (62,63). Although a previous report showed that CVB3 infection caused the generation of mtROS, NAC treatment, which blocks the generation of cytosolic ROS, did not inhibit CVB3 replication (64). Similarly, we confirmed that NAC did not inhibit CVB3 replication *in vitro*. NAC may only partially decrease mtROS generation and was not sufficient to diminish the effects of mtROS (65).

CAR is a transmembrane protein of the immunoglobulin superfamily and is involved in cell adhesion, thereby mediating the entry of CVB3 into host cells (66). In the current study, we found that CAR expression increased in cells upon OA treatment and that treatment of cells with valsartan reduced CAR expression. A previous report showed that valsartan-induced CAR downregulation decreased coxsackievirus infection in human endothelial cells (25). However, our data showed that valsartan did not significantly inhibit CVB3 replication in OA-

treated Vero cells, suggesting that the enhanced susceptibility of CVB3 in OA treatment may not be related to increased CAR expression upon OA treatment.

Although we sought to identify the mechanisms through which lipid accumulation increases viral replication in CVB3 infection, we were unable to determine the direct effects of mtROS through RO formation. Therefore, further studies are needed to establish the specific mechanisms through which accumulated lipids and increased mtROS directly affect viral replication in cells.

OA treatment increases lipid droplet formation in cells (48), and which induces mtROS generation. The formation of MDVs is increased by oxidative stress (67), and it transfers membrane components and mitochondrial contents including mtDNA to MVB (26). Increase of CVB3 replication in ROs was observed in cells with elevated mtROS levels, and inhibition of mtROS suppressed CVB3 replication. These results suggest that lipid-induced mtROS increase viral replication, presumably by increasing MDV formation (**Supplementary Fig. 4**).

In summary, we found that CVB3 infection increased with obesity. OA treatment aggravated CVB3 infection *in vitro* because of increased mtROS production. We showed that the treatment of MitoQ inhibited mortality induced by CVB3 infection in HFD-fed mice and suggest that mtROS inhibitors act as potential therapeutic agents against severely increased CVB3 infection caused by obesity. In addition, this study suggests that mitochondrial changes related to fat metabolism are associated with enhanced viral infection and are expected to be applied in the development of new strategies to fight viral infection in the future.

ACKNOWLEDGEMENTS

SUPPLEMENTARY MATERIALS

Supplementary Figure 1
Histopathological analysis of the pancreas, heart, and liver from CVB3-infected HFD-induced obese mice. Mice were fed a RD and/or HFD for 4 weeks. Mice were intraperitoneally infected with CVB3 (1×10^6 pfu/mouse). (A) H&E staining of the pancreas at 1–3 days post-infection. H&E staining of (B) liver and (C) heart tissues at 3 days post-infection.

Click here to view

Supplementary Figure 2
OA increased CVB3 amounts in Vero cell. The RT-qPCR assays were carried out in 20 μL of a reaction mixture comprising 5 μL of extracted RNA and 15 μL of D.W. AccuPower® Enterovirus customized Real Time RT-PCR Kit (Bioneer Corp., Daejeon, Korea) was used for

the quantification. RT-PCR amplification were run in a Quantstudio 5 system (Thermo Fisher Scientific, Inc., Waltham, MA, USA) under the following the conditions: 50°C for 30 min at reverse transcription, 95°C at 10 min for initial denaturation then followed by 45 cycles of amplification with denaturation at 95°C for 15 s and annealing and extension at 55°C for 30 s. A standard curve was generated using 10-fold serial dilution (10^7 to 10^3 copy/test of *in vitro* transcript RNA).

Click here to view

Supplementary Figure 3

NAC did not attenuate cytotoxicity increased by OA treatment in CVB3-infected Vero cells. Vero cells were pretreated with 100 μM OA in 0.1% BSA for 24 h and subsequently infected with CCVB3 at a MOI of 10 in the presence or absence of 10 mM NAC for 48 h. (A) Viability of Vero cells was measured using SRB assays. All figures are representative examples of experiments performed in triplicate. Data are expressed as means±SEMs.

Click here to view

Supplementary Figure 4

Lipid-induced mitochondrial ROS increased viral replication.

Click here to view

REFERENCES

1. Stefan N, Birkenfeld AL, Schulze MB, Ludwig DS. Obesity and impaired metabolic health in patients with COVID-19. *Nat Rev Endocrinol* 2020;16:341-342.
   PUBMED | CROSSREF

2. Karjala Z, Neal D, Rohrer J. Association between HSV1 seropositivity and obesity: data from the National Health and Nutritional Examination Survey, 2007–2008. *PLoS One* 2011;6:e19092.
   PUBMED | CROSSREF

3. Honce R, Schultz-Cherry S. Impact of obesity on influenza a virus pathogenesis, immune response, and evolution. *Front Immunol* 2019;10:1071.
   PUBMED | CROSSREF

4. Fairweather D, Stafford KA, Sung YK. Update on coxsackievirus B3 myocarditis. *Curr Opin Rheumatol* 2012;24:401-407.
   PUBMED | CROSSREF

5. Huber S, Ramsingh AI. Coxsackievirus-induced pancreatitis. *Viral Immunol* 2004;17:358-369.
   PUBMED | CROSSREF

6. Pedersen KW, van der Meer Y, Roos N, Snijder EJ. Open reading frame 1a-encoded subunits of the arterivirus replicase induce endoplasmic reticulum-derived double-membrane vesicles which carry the viral replication complex. *J Virol* 1999;73:2016-2026.
   PUBMED | CROSSREF

7. Limpens RW, van der Schaar HM, Kumar D, Koster AJ, Snijder EJ, van Kuppeveld FJ, Bárcena M. The transformation of enterovirus replication structures: a three-dimensional study of single- and double-membrane compartments. *MBio* 2011;2:e00166-11.
   PUBMED | CROSSREF

8. Knoops K, Kikkert M, Worm SH, Zevenhoven-Dobbe JC, van der Meer Y, Koster AJ, Mommaas AM, Snijder EJ. SARS-coronavirus replication is supported by a reticulovesicular network of modified endoplasmic reticulum. *PLoS Biol* 2008;6:e226.
   PUBMED | CROSSREF

9. Liu Z, Ren Z, Zhang J, Chuang CC, Kandaswamy E, Zhou T, Zuo L. Role of ros and nutritional antioxidants in human diseases. *Front Physiol* 2018;9:477.
   PUBMED | CROSSREF

10. Guillin OM, Vindry C, Ohlmann T, Chavatte L. Selenium, selenoproteins and viral infection. *Nutrients* 2019;11:2101.
    PUBMED | **CROSSREF**

11. Chi J, Yu S, Liu C, Zhao X, Zhong J, Liang Y, Ta N, Yin X, Zhao D. Nox4-dependent ROS production is involved in CVB$_3$-induced myocardial apoptosis. *Biochem Biophys Res Commun* 2018;503:1641-1644.
    PUBMED | **CROSSREF**

12. Wang Y, Gao B, Xiong S. Involvement of NLRP3 inflammasome in CVB3-induced viral myocarditis. *Am J Physiol Heart Circ Physiol* 2014;307:H1438-H1447.
    PUBMED | **CROSSREF**

13. To EE, Erlich JR, Liong F, Luong R, Liong S, Esaq F, Oseghale O, Anthony D, McQualter J, Bozinovski S, et al. Mitochondrial reactive oxygen species contribute to pathological inflammation during influenza a virus infection in mice. *Antioxid Redox Signal* 2020;32:929-942.
    PUBMED | **CROSSREF**

14. Li J, Ma C, Long F, Yang D, Liu X, Hu Y, Wu C, Wang B, Wang M, Chen Y, et al. Parkin impairs antiviral immunity by suppressing the mitochondrial reactive oxygen species-nlrp3 axis and antiviral inflammation. *iScience* 2019;16:468-484.
    PUBMED | **CROSSREF**

15. Sreekanth GP, Panaampon J, Suttitheptumrong A, Chuncharunee A, Bootkunha J, Yenchitsomanus PT, Limjindaporn T. Drug repurposing of N-acetyl cysteine as antiviral against dengue virus infection. *Antiviral Res* 2019;166:42-55.
    PUBMED | **CROSSREF**

16. Hu M, Bogoyevitch MA, Jans DA. Subversion of host cell mitochondria by RSV to favor virus production is dependent on inhibition of mitochondrial complex I and ROS generation. *Cells* 2019;8:1417.
    PUBMED | **CROSSREF**

17. Hong EH, Song JH, Kim SR, Cho J, Jeong B, Yang H, Jeong JH, Ahn JH, Jeong H, Kim SE, et al. Morin hydrate inhibits influenza virus entry into host cells and has anti-inflammatory effect in influenza-infected mice. *Immune Netw* 2020;20:e32.
    PUBMED | **CROSSREF**

18. Kim SR, Song JH, Ahn JH, Lee GS, Ahn H, Yoon SI, Kang SG, Kim PH, Jeon SM, Choi EJ, et al. Antiviral and anti-inflammatory activity of budesonide against human rhinovirus infection mediated via autophagy activation. *Antiviral Res* 2018;151:87-96.
    PUBMED | **CROSSREF**

19. Shi H, Bartness TJ. White adipose tissue sensory nerve denervation mimics lipectomy-induced compensatory increases in adiposity. *Am J Physiol Regul Integr Comp Physiol* 2005;289:R514-R520.
    PUBMED | **CROSSREF**

20. Henke A, Launhardt H, Klement K, Stelzner A, Zell R, Munder T. Apoptosis in coxsackievirus B3-caused diseases: interaction between the capsid protein VP2 and the proapoptotic protein siva. *J Virol* 2000;74:4284-4290.
    PUBMED | **CROSSREF**

21. Limsuwat N, Boonarkart C, Phakaratsakul S, Suptawiwat O, Auewarakul P. Influence of cellular lipid content on influenza A virus replication. *Arch Virol* 2020;165:1151-1161.
    PUBMED | **CROSSREF**

22. Dias SSG, Soares VC, Ferreira AC, Sacramento CQ, Fintelman-Rodrigues N, Temerozo JR, Teixeira L, Nunes da Silva MA, Barreto E, Mattos M, et al. Lipid droplets fuel SARS-CoV-2 replication and production of inflammatory mediators. *PLoS Pathog* 2020;16:e1009127.
    PUBMED | **CROSSREF**

23. Burckhardt CJ, Suomalainen M, Schoenenberger P, Boucke K, Hemmi S, Greber UF. Drifting motions of the adenovirus receptor CAR and immobile integrins initiate virus uncoating and membrane lytic protein exposure. *Cell Host Microbe* 2011;10:105-117.
    PUBMED | **CROSSREF**

24. Serrano M, Moreno M, Bassols J, Moreno-Navarrete JM, Ortega F, Ricart W, Fernández-Real JM. Coxsackie and adenovirus receptor is increased in adipose tissue of obese subjects: a role for adenovirus infection? *J Clin Endocrinol Metab* 2015;100:1156-1163.
    PUBMED | **CROSSREF**

25. Funke C, Farr M, Werner B, Dittmann S, Überla K, Piper C, Niehaus K, Horstkotte D. Antiviral effect of Bosentan and Valsartan during coxsackievirus B3 infection of human endothelial cells. *J Gen Virol* 2010;91:1959-1970.
    PUBMED | **CROSSREF**

26. Soto-Heredero G, Baixauli F, Mittelbrunn M. Interorganelle communication between mitochondria and the endolysosomal system. *Front Cell Dev Biol* 2017;5:95.
    PUBMED | **CROSSREF**

27. Sugiura A, McLelland GL, Fon EA, McBride HM. A new pathway for mitochondrial quality control: mitochondrial-derived vesicles. *EMBO J* 2014;33:2142-2156.
    PUBMED | CROSSREF

28. Picca A, Guerra F, Calvani R, Coelho-Junior HJ, Bossola M, Landi F, Bernabei R, Bucci C, Marzetti E. Generation and release of mitochondrial-derived vesicles in health, aging and disease. *J Clin Med* 2020;9:1440.
    PUBMED | CROSSREF

29. Burgyan J, Rubino L, Russo M. The 5′-terminal region of a tombusvirus genome determines the origin of multivesicular bodies. *J Gen Virol* 1996;77:1967-1974.
    PUBMED | CROSSREF

30. Bass VL, Soukup JM, Ghio AJ, Madden MC. Oleic acid and derivatives affect human endothelial cell mitochondrial function and vasoactive mediator production. *Lipids Health Dis* 2020;19:128.
    PUBMED | CROSSREF

31. Bozi LH, Bechara LR, Dos Santos AF, Campos JC. Mitochondrial-derived vesicles: a new player in cardiac mitochondrial quality control. *J Physiol* 2016;594:6077-6078.
    PUBMED | CROSSREF

32. Neuspiel M, Schauss AC, Braschi E, Zunino R, Rippstein P, Rachubinski RA, Andrade-Navarro MA, McBride HM. Cargo-selected transport from the mitochondria to peroxisomes is mediated by vesicular carriers. *Curr Biol* 2008;18:102-108.
    PUBMED | CROSSREF

33. Cadete VJ, Deschênes S, Cuillerier A, Brisebois F, Sugiura A, Vincent A, Turnbull D, Picard M, McBride HM, Burelle Y. Formation of mitochondrial-derived vesicles is an active and physiologically relevant mitochondrial quality control process in the cardiac system. *J Physiol* 2016;594:5343-5362.
    PUBMED | CROSSREF

34. Li B, Zhao H, Wu Y, Zhu Y, Zhang J, Yang G, Yan Q, Li J, Li T, Liu L. Mitochondrial-derived vesicles protect cardiomyocytes against hypoxic damage. *Front Cell Dev Biol* 2020;8:214.
    PUBMED | CROSSREF

35. Gremmels H, Bevers LM, Fledderus JO, Braam B, van Zonneveld AJ, Verhaar MC, Joles JA. Oleic acid increases mitochondrial reactive oxygen species production and decreases endothelial nitric oxide synthase activity in cultured endothelial cells. *Eur J Pharmacol* 2015;751:67-72.
    PUBMED | CROSSREF

36. Cheng ML, Weng SF, Kuo CH, Ho HY. Enterovirus 71 induces mitochondrial reactive oxygen species generation that is required for efficient replication. *PLoS One* 2014;9:e113234.
    PUBMED | CROSSREF

37. Bond ST, Kim J, Calkin AC, Drew BG. The antioxidant moiety of mitoq imparts minimal metabolic effects in adipose tissue of high fat fed mice. *Front Physiol* 2019;10:543.
    PUBMED | CROSSREF

38. Ghilotti F, Bellocco R, Ye W, Adami HO, Trolle Lagerros Y. Obesity and risk of infections: results from men and women in the Swedish National March Cohort. *Int J Epidemiol* 2019;48:1783-1794.
    PUBMED | CROSSREF

39. Falagas ME, Kompoti M. Obesity and infection. *Lancet Infect Dis* 2006;6:438-446.
    PUBMED | CROSSREF

40. Kwok S, Adam S, Ho JH, Iqbal Z, Turkington P, Razvi S, Le Roux CW, Soran H, Syed AA. Obesity: a critical risk factor in the COVID-19 pandemic. *Clin Obes* 2020;10:e12403.
    PUBMED | CROSSREF

41. Torres L, Martins VD, Faria AMC, Maioli TU. The intriguing relationship between obesity and infection. *J Infect (Grand Rapids)* 2018;1:6-10.
    CROSSREF

42. Namkoong H, Ishii M, Fujii H, Asami T, Yagi K, Suzuki S, Azekawa S, Tasaka S, Hasegawa N, Betsuyaku T. Obesity worsens the outcome of influenza virus infection associated with impaired type I interferon induction in mice. *Biochem Biophys Res Commun* 2019;513:405-411.
    PUBMED | CROSSREF

43. Gebhard JR, Perry CM, Harkins S, Lane T, Mena I, Asensio VC, Campbell IL, Whitton JL. Coxsackievirus B3-induced myocarditis: perforin exacerbates disease, but plays no detectable role in virus clearance. *Am J Pathol* 1998;153:417-428.
    PUBMED | CROSSREF

44. Daley AJ, Isaacs D, Dwyer DE, Gilbert GL. A cluster of cases of neonatal coxsackievirus B meningitis and myocarditis. *J Paediatr Child Health* 1998;34:196-198.
    PUBMED | CROSSREF

45. Wolff G, Melia CE, Snijder EJ, Bárcena M. Double-membrane vesicles as platforms for viral replication. *Trends Microbiol* 2020;28:1022-1033.
   PUBMED | **CROSSREF**

46. Cook GW, Benton MG, Akerley W, Mayhew GF, Moehlenkamp C, Raterman D, Burgess DL, Rowell WJ, Lambert C, Eng K, et al. Structural variation and its potential impact on genome instability: novel discoveries in the EGFR landscape by long-read sequencing. *PLoS One* 2020;15:e0226340.
   PUBMED | **CROSSREF**

47. Peters CE, Carette JE. Return of the neurotropic enteroviruses: co-opting cellular pathways for infection. *Viruses* 2021;13:166.
   PUBMED | **CROSSREF**

48. Ormseth MJ, Swift LL, Fazio S, Linton MF, Raggi P, Solus JF, Oeser A, Bian A, Gebretsadik T, Shintani A, et al. Free fatty acids are associated with metabolic syndrome and insulin resistance but not inflammation in systemic lupus erythematosus. *Lupus* 2013;22:26-33.
   PUBMED | **CROSSREF**

49. Muro E, Atilla-Gokcumen GE, Eggert US. Lipids in cell biology: how can we understand them better? *Mol Biol Cell* 2014;25:1819-1823.
   PUBMED | **CROSSREF**

50. Molteni CG, Principi N, Esposito S. Reactive oxygen and nitrogen species during viral infections. *Free Radic Res* 2014;48:1163-1169.
   PUBMED | **CROSSREF**

51. Camini FC, da Silva TF, da Silva Caetano CC, Almeida LT, Ferraz AC, Alves Vitoreti VM, de Mello Silva B, de Queiroz Silva S, de Magalhães JC, de Brito Magalhães CL. Antiviral activity of silymarin against Mayaro virus and protective effect in virus-induced oxidative stress. *Antiviral Res* 2018;158:8-12.
   PUBMED | **CROSSREF**

52. Paul D, Hoppe S, Saher G, Krijnse-Locker J, Bartenschlager R. Morphological and biochemical characterization of the membranous hepatitis C virus replication compartment. *J Virol* 2013;87:10612-10627.
   PUBMED | **CROSSREF**

53. Melia CE, van der Schaar HM, Lyoo H, Limpens RW, Feng Q, Wahedi M, Overheul GJ, van Rij RP, Snijder EJ, Koster AJ, et al. Escaping host factor pi4kb inhibition: Enterovirus genomic RNA replication in the absence of replication organelles. *Cell Reports* 2017;21:587-599.
   PUBMED | **CROSSREF**

54. Soubannier V, McLelland GL, Zunino R, Braschi E, Rippstein P, Fon EA, McBride HM. A vesicular transport pathway shuttles cargo from mitochondria to lysosomes. *Curr Biol* 2012;22:135-141.
   PUBMED | **CROSSREF**

55. Abuaita BH, Schultz TL, O'Riordan MX. Mitochondria-derived vesicles deliver antimicrobial reactive oxygen species to control phagosome-localized staphylococcus aureus. *Cell Host Microbe* 2018;24:625-636.e5.
   PUBMED | **CROSSREF**

56. Uchil P, Mothes W. Viral entry: a detour through multivesicular bodies. *Nat Cell Biol* 2005;7:641-642.
   PUBMED | **CROSSREF**

57. Chu H, Wang JJ, Spearman P. Human immunodeficiency virus type-1 gag and host vesicular trafficking pathways. *Curr Top Microbiol Immunol* 2009;339:67-84.
   PUBMED | **CROSSREF**

58. Kelso GF, Porteous CM, Coulter CV, Hughes G, Porteous WK, Ledgerwood EC, Smith RA, Murphy MP. Selective targeting of a redox-active ubiquinone to mitochondria within cells: antioxidant and antiapoptotic properties. *J Biol Chem* 2001;276:4588-4596.
   PUBMED | **CROSSREF**

59. Kelso GF, Porteous CM, Hughes G, Ledgerwood EC, Gane AM, Smith RA, Murphy MP. Prevention of mitochondrial oxidative damage using targeted antioxidants. *Ann N Y Acad Sci* 2002;959:263-274.
   PUBMED | **CROSSREF**

60. Smith RA, Porteous CM, Gane AM, Murphy MP. Delivery of bioactive molecules to mitochondria in vivo. *Proc Natl Acad Sci U S A* 2003;100:5407-5412.
   PUBMED | **CROSSREF**

61. Weiss L, Hildt E, Hofschneider PH. Anti-hepatitis B virus activity of N-acetyl-L-cysteine (NAC): new aspects of a well-established drug. *Antiviral Res* 1996;32:43-53.
   PUBMED | **CROSSREF**

62. Gaudernak E, Seipelt J, Triendl A, Grassauer A, Kuechler E. Antiviral effects of pyrrolidine dithiocarbamate on human rhinoviruses. *J Virol* 2002;76:6004-6015.
   PUBMED | **CROSSREF**

63. Schweizer M, Peterhans E. Oxidative stress in cells infected with bovine viral diarrhoea virus: a crucial step in the induction of apoptosis. *J Gen Virol* 1999;80:1147-1155.
   PUBMED | **CROSSREF**

64. Si X, McManus BM, Zhang J, Yuan J, Cheung C, Esfandiarei M, Suarez A, Morgan A, Luo H. Pyrrolidine dithiocarbamate reduces coxsackievirus B3 replication through inhibition of the ubiquitin-proteasome pathway. *J Virol* 2005;79:8014-8023.
   PUBMED | **CROSSREF**

65. Wang Z, Cai F, Chen X, Luo M, Hu L, Lu Y. The role of mitochondria-derived reactive oxygen species in hyperthermia-induced platelet apoptosis. *PLoS One* 2013;8:e75044.
   PUBMED | **CROSSREF**

66. Marchant D, Si X, Luo H, McManus B, Yang D. The impact of CVB3 infection on host cell biology. *Curr Top Microbiol Immunol* 2008;323:177-198.
   PUBMED | **CROSSREF**

67. Perna AF, Violetti E, Lanza D, Sepe I, Bellinghieri G, Savica V, Santoro D, Satta E, Cirillo G, Lupo A, et al. Therapy of hyperhomocysteinemia in hemodialysis patients: effects of folates and N-acetylcysteine. *J Ren Nutr* 2012;22:507-514.e1.
   PUBMED | **CROSSREF**